ELSEVIER

Contents lists available at ScienceDirect

Cement and Concrete Composites

journal homepage: www.elsevier.com/locate/cemconcomp



Scale-linking model of self-healing and stiffness recovery in Engineered Cementitious Composites (ECC)



Hui Ma^{a,b}, Emily Herbert^c, Motohiro Ohno^d, Victor C. Li^{c,*}

- ^a School of Materials Science and Engineering, Southeast University, Nanjing 210096, PR China
- ^b Jiangsu Expressway Engineering Maintenance Technology Co. Ltd, Nanjing 210096, PR China
- ^c Department of Civil and Environmental Engineering, University of Michigan, 2326 G.G. Brown Building, Ann Arbor, MI 48109, USA
- ^d Department of Civil Engineering, The University of Tokyo, 7-3-1 Hongo, Bunkyo-ku, Tokyo, Japan

ARTICLE INFO

Keywords: Engineered Cementitious Composites (ECC) Self-healing Stiffness recovery Crack patterns Scale-linking model

ABSTRACT

Micro-crack damage in Engineered Cementitious Composites (ECC) has demonstrated self-repairing capacity when exposed to wetting-drying cycles. Previous studies qualitatively relate composite stiffness recovery to crack width. There is a need to develop a more quantitative understanding of the relationship between the magnitude of self-healing and imposed strain in ECC. An analytic model that links the stiffness recovery of a single crack in ECC (meso-scale) to that of an ECC loaded to multiple micro-crack damage (macro-scale) was investigated in this study. The objective of this research is to develop this theoretical scale-linking model and validate it with experimental data. It is found that the proposed scale-linking model successfully predicted the composite stiffness recovery at any strain, based on known macro-scale crack patterns and meso-scale self-healing behavior. It is concluded that the new model captures the essence of self-healing behavior in ECC. The model clarifies the pathway for designing ECC with robust self-healing behavior.

1. Introduction

Cracking is one of the major forms of damages of concrete structures during their service lives. Cracks can be caused by many factors, such as loading, temperature changes, shrinkage, alkali-silicate reactions, and freezing/thawing cycles [1]. Cracks have significantly negative impacts on the mechanical properties of concrete materials, and thus weaken concrete structures. The presence of cracks also reduces the durability of concrete structures via creating preferential paths for harmful agents to penetrate the structure and attack the surrounding concrete. Reinforcement may also be damaged through corrosion when exposed to these harmful agents [2]. Therefore, developing a cementitious material that can heal these cracks automatically is highly desirable for structural resiliency and durability.

The self-healing phenomenon of cementitious materials, commonly known as autogenous healing, has been observed in natural environments for many years. One such example, which was observed by the French Academy of Science in 1836, is the action of small cracks in a concrete bridge healing themselves by recrystallization of calcite in the presence of moisture [3]. Since then, extensive studies had been conducted on the self-healing behavior of cementitious materials as overviewed in Ref. [4,5]. Experimental investigations and practical

experiences demonstrated that the healing of cracks in cementitious materials leads to a gradual reduction of permeability over time when exposed to flowing water [6,7]. Studies [8,9,10] indicate that the self-healing functionality is mainly attributed to the formation of calcium carbonate as a result of the reaction between the calcium ions in concrete and the atmospheric carbon dioxide dissolved in the water flowing through the cracks. Continuous hydration of un-hydrated cementitious materials is another intrinsic mechanism of self-healing [9,11,12]. However, due to the limited quantity of self-healing products, the self-healing capacity of cementitious materials is strongly affected by crack width. In previous studies [7,13], complete healing was shown to occur in cracks less than 150 μ m in width, which is very difficult to achieve in brittle concrete materials, even with steel reinforcements.

Engineered Cementitious Composites (ECC), a special kind of High Performance Fiber Reinforced Cementitious Composites (HPFRCC), was developed by Li and coworkers in the 1990s [14]. It contains randomly oriented short fibers with a moderate volume fraction of 1.5–2%. The unique characteristics of ECC materials are the high tensile ductility and tight multiple cracks. ECC possess extreme tensile ductility of 2–8% (200–800 times that of normal concrete or FRC), and their average maximum crack width is approximately $60\,\mu m$, even in highly strained

E-mail address: vcli@umich.edu (V.C. Li).

^{*} Corresponding author.

states [15] [16,17]. In addition, unlike normal concrete and fiber reinforced concrete materials, the tight crack width in ECC is an intrinsic material property, independent of structural size, steel reinforcement, or the load applied to a structure built with ECC materials. Owing to these characteristics, ECC is considered a promising candidate for self-healing concrete material.

Many previous studies have demonstrated that microcrack damaged ECC materials are able to recover transport and mechanical properties through self-healing behavior. Under wet-dry cycles, permeability tests indicated that flow rate of water through a cracked ECC specimen under a fixed pressure reduced gradually, and reduced to zero after 10 healing cycles [10]. Further, the permeability of ECC specimens with crack widths below 50 µm was found to be identical to that of virgin uncracked specimens [18]. Resonant frequency of cracked ECC after 10 wet-dry cycles can recover to over 90% that of the undamaged specimen, even at a 2.0% preloading strain [19]. In addition, self-healing behavior of ECC is not limited to a controlled laboratory environment, but can also occur in the natural environment [20].

Most previous studies focused on the effects of ECC's self-healing behavior at the macro-scale composite properties (mechanical and transport properties). Numerical modelling have been conducted to simulate/predict the self-healing behavior. Hilloulin et al. [21,22] proposed hydro-chemo-mechanical model and comprehensive finite element model to evaluate the mechanical properties of the healing products in ultra-high performance concrete (UHPC) material. Aliko-Benitez et al. [23] developed an a physicochemical based model of healing activated by precipitation of calcium carbonate inside concrete cracks. Davies and Jefferson proposed a model using a 3D two phase micro-mechanical constitutive formulation, which successfully simulated the recovery of mechanical properties of cementitious materials [24]. Caggiano et al. [25] proposed a zero-thickness interface formulation for self-healing concrete, with self-healing effects modeled by a calibrated time evolution of the concrete open porosity. Recently a modified SMM (solidification-Microprestress-Microplane) model was proposed by Di Luzio et al. [26], which properly describes the selfhealing of a cementitious material in terms of the recovery of load bearing capacity.

These models are focused on the physio-chemistry and micro-mechanical properties of self-healing products in cementitious materials. There has been no research to quantitatively relate the knowledge and findings on self-healing at the meso-scale to that at the macro-scale which includes typically a distribution of cracks with varying widths. Therefore, in order to fill the knowledge gap and systematically understand the self-healing behavior of ECC materials that strain-hardens with multiple cracks (Fig. 1), an investigation linking the self-healing induced property recovery on a single crack to that on the composite scale is necessary.

In this study, a scale-linking analytic model is developed and experimentally verified. Specifically, the stiffness recovery of ECC under tensile loading in the meso single-crack scale and that at the macro composite-scale were investigated experimentally. In addition, the crack patterns (including crack width and number) on ECC were observed at various tensile strains. The crack width distribution (CWD) was then best-fitted and mathematically expressed by probability



Fig. 1. The multiple crack pattern of ECC material under tensile loading.

density function (PDF). It is hypothesized that self-healing induced composite stiffness recovery is a direct result of stiffness recovery of individual cracks and that the extent of composite healing reflects the distribution of crack widths that strongly (and non-linearly) governs the healing of a crack in ECC. The scale-linking model was used to predict the ECC composite's (macro-scale) stiffness recovery at various tensile strains based on the stiffness recovery of single crack (meso-scale) and PDF of crack width distribution. The objective of this research is to establish and verify a theoretical model that links macro-scale stiffness recovery to meso-scale stiffness recovery due to self-healing. Although this phenomenological model does not describe the physio-chemical mechanisms of self-healing, it none-the-less elevates the behavior of self-healing from the meso to the macro-scale, provided the crack pattern is known from laboratory direct tension tests. Thus, this model can be employed to estimate the extent of self-healing in different parts of a structure with known distribution of crack damage strain, at least for the wet-dry exposure condition used in this study.

2. Research significance and framework

This study, for the first time, investigates and relates the self-healing behaviors of ECC on multi-scales. Although many previous studies on the self-healing behaviors of ECC materials have been conducted, a holistic understanding of ECC's self-healing on multi-scales is absent. The lack of systematic knowledge slows the development of robust self-healing performance of ECC materials and limits their reliable application in the field. Therefore, this study proposes an analytical scale-linking model correlating the ECC's self-healing on meso- and macroscales. With this model, the ECC's self-healing behavior (stiffness recovery) can be predicted at any imposed composite strain. Significant contributions of this study also include the meso-scale insights into the stiffness recovery of single crack specimens after self-healing and its analytical scale-linking to the macro-scale stiffness recovery of ECC.

In developing the scale-linking model, two major assumptions were adopted: 1) The degree of stiffness recovery of a single crack is uniquely determined by its crack width, under given material, loading, and environmental (exposure) conditions; 2) CWD of ECC specimens follows a specific probability distribution characterized by the imposed strain level, for a given ECC composition. Based on the first assumption, the stiffness recovery of single crack r_E can be described as a function of crack width δ . The second hypothesis implies that CWD of ECC specimens under loading can be characterized by a PDF $p(\delta,\epsilon)$ parameterized by the tensile strain level ϵ . Coupling the stiffness recovery of single crack r_E and PDF $p(\delta,\epsilon)$, the stiffness recovery of ECC composites R_E at a given strain level can be predicted through the analytical scale-linking model.

The research framework of this study is shown in Fig. 2. On the macro-scale, the PDFs $p(\delta, \varepsilon)$ of CWDs on the surface of ECC specimens at various strains were obtained experimentally. On the meso-scale, the stiffness recoveries of single cracked ECC specimens as a function of crack width $r_E(\delta)$ were experimentally investigated. With this information from the meso- and macro-scales, the scale-linking model $R_E(\varepsilon) = f[r_E(\delta), \ p(\delta, \varepsilon)]$ was analytically formulated to predict the stiffness recovery of ECC composites at any tensile strain. Concurrently, the stiffness recoveries of ECC composites were investigated experimentally, and were then used to verify the analytical scale-linking model. The present research parallels a similar scale-linking approach used to predict the composite electrical resistivity and water permeability of ECC based on those of single crack specimens [27,28].

3. Experimental investigations

3.1. Raw materials and specimen preparation

The ECC mixture proportions used in this study are given in Table 1. In order to verify the applicability of analytical scale-linking model for

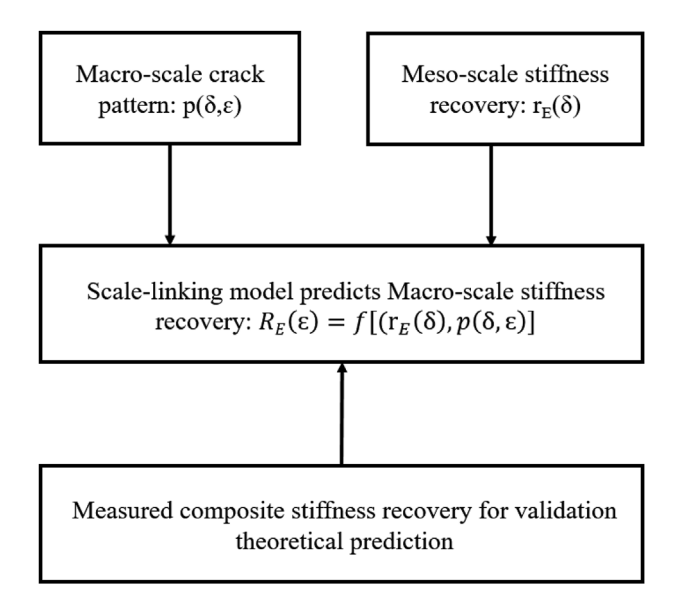


Fig. 2. The proposed scale-linking model integrates information on stiffness recovery of a single crack r_E at given crack opening δ and the CWD curve $p(\delta)$ at a given strain ϵ to compute the composite scale stiffness recovery $R_E(\epsilon)$ of any given ECC, which is verified by measurement of composite stiffness recovery.

Table 1Mix proportions of ECC mixtures (weight fraction).

ECC Mixture	Cement	Fly ash	Silica sand	HRWRA	Water	PVA fiber ^a
ECC-1	1	1.2	0.8	0.013	0.58	2%
ECC-2	1	2.2	1.16	0.013	0.8	2%

^a PVA fibers were added by volume of total ECC mixture.

ECC with different mixture proportions, two ECC mixtures were prepared in this study. For ECC-1 and ECC-2, the fly ash to cement ratio was 1.2 and 2.2, respectively. The raw materials include Type I Portland cement, Class F fly ash, fine silica sand with an average particle size of 110 µm, water, and polyvinyl-alcohol (PVA) fiber (produced by Kuraray Co. Ltd.). In order to adjust the workability of the ECC mixtures, a polycarboxylate-based high range water reducing admixture (HRWRA) was also used. The PVA fibers were 12 mm in length with a diameter of $39\,\mu m$, and had a tensile strength of $1620\,MPa$, a density of 1.3 g/cm³, an elastic modulus of 42.8 GPa, and a maximum elongation of 7%. The fibers account for 2% of the total ECC mixture volume. The surface of the fibers was coated with an oiling agent, which amounted to 1.2% by weight of fiber, to reduce the interfacial chemical bond between the fiber and matrix caused by the strong hydrophilic nature of the PVA fiber, in order to meet the conditions for composite tensile strain-hardening [29,30].

All ECC mixtures were prepared following the typical production procedures [31]. The raw materials were mixed in a 20 L force-based Hobart mixer, and the fresh mixture was cast into molds. The dog-bone shaped specimens were prepared as recommended by the Japan Society of Civil Engineers (JSCE) [32] for testing ductile concretes, and the detailed dimensions are shown in Fig. 3. All specimens were covered with plastic sheeting for 24 h until demolding, and then cured in room temperature conditions, with a temperature of 20 \pm 2 °C and relative humidity of 50 \pm 5%, until the predetermined testing age of 28 days.

3.2. Experimental procedures

3.2.1. Crack pattern observations

In order to investigate the crack patterns (crack width and number) of ECC at various strains, the uniaxial tensile test (Fig. 4) was conducted on dog-bone specimens. The test was conducted using a 50 kN capacity

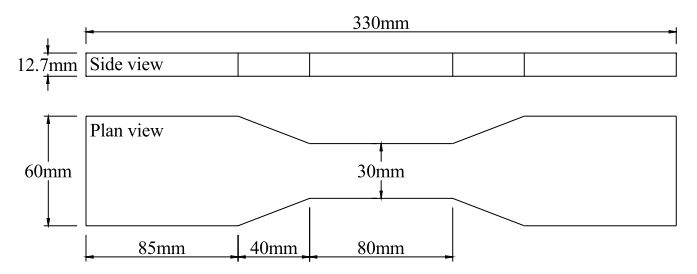


Fig. 3. Dimensions of dog-bone shaped specimens.



Fig. 4. Uniaxial tensile test setup on dog-bone specimen.

load frame (Instron Model 5969) under displacement control at a rate of 0.5 mm/min as recommended by JSCE for direct tension testing of high performance fiber reinforced cementitious composites [32]. Two Linear Variable Displacement Transducers (LVDTs) were attached to both sides of the specimen to measure tensile deformation.

Depending on the ultimate tensile strain capacity, the dog-bone specimens of ECC-1 and ECC-2 were preloaded to 0.25%, 0.35%, 0.5%, 0.75% and 1% tensile strain, and 0.5%, 0.8%, 1.0%, 1.2%, 1.5%, 1.8% and 2.0% tensile strain, respectively. The different maximum imposed strains for ECC-1 and ECC-2 reflect the different strain capacities of these two mixes. From past experience, it is known that ECC with higher amount of fly ash tends to have a larger tensile strain capacity. Representative tensile stress-strain curves for each ECC mix are shown in Fig. 5. Six specimens were tested for each mix at each strain level. Once the desired strain was reached, the specimen was removed from the load frame, and each crack width was measured and counted using a handheld optical microscope. Since the resolution of the microscope is $10 \, \mu m$, cracks with width less than $10 \, \mu m$ were not included in the data set. In addition, due to the limited measurement accuracy of the optical microscope, crack width data was measured and recorded in intervals of 10 µm. The crack patterns of these two ECC materials at various strains were then determined and analyzed.

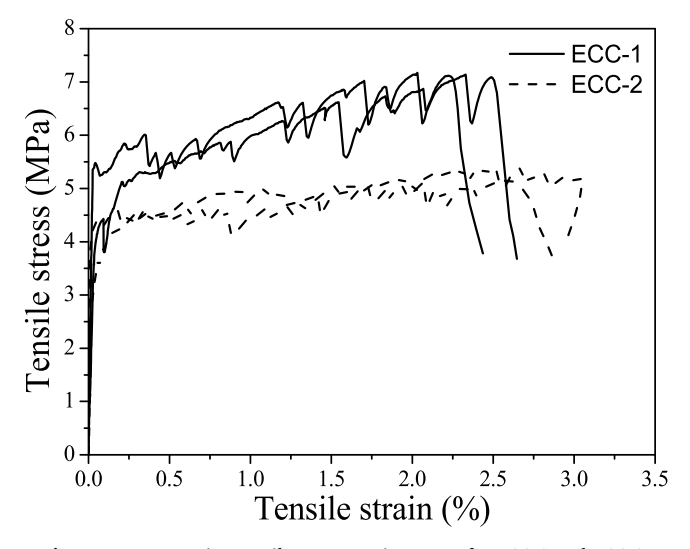


Fig. 5. Representative tensile stress-strain curves for ECC-1 and ECC-2.

3.2.2. Stiffness recovery of composite

In order to verify the scale-linking model proposed in this study, the stiffness recovery of the ECC mixtures were experimentally determined. The preloaded specimens in Section 3.2.1 were exposed to wet-dry cyclical conditions for self-healing. According to the report of Zhang [33], the stiffness recovery of unhealed specimen is almost zero, which coincides with the experience of the authors. Therefore, the unhealed specimens were not investigated in this study. Each wetting-drying cycle consisted of 24 h submerged in water, followed by 24 h of drying in laboratory air [10] [12]. After 10 healing cycles, the specimens were reloaded until failure. The secant stiffness, between the origin and first cracking strength, during preloading (Stiffness_{preloading}) and reloading (Stiffness_{reloading}) was measured. The stiffness recovery was then calculated as:

$$R_{E}(\varepsilon) = \frac{Stiffness_{reloading}}{Stiffness_{preloading}} \times 100\%$$
(1)

3.2.3. Stiffness recovery of single crack

In order to investigate how stiffness recovery varies with crack width, uniaxial tensile tests were conducted on notched dog-bone specimens. The notch was cut in the middle of the dog-bone specimens using a precision saw. The detailed dimensions of notched dog-bone specimens are shown in Fig. 6. The notches were 1 mm in width, 6 mm in depth on the sides of the specimens, and 2 mm in depth on the front and back of the specimens. The notch thickness (1 mm) selected in this study was efficient for producing one single crack [34].

The single crack was produced in the notched section through uniaxial tension following the suggested procedure in Ref. [35], as shown in Fig. 7. As can be seen, two LVDTs were attached on both sides of the specimen to measure the extension, treated as the width of a

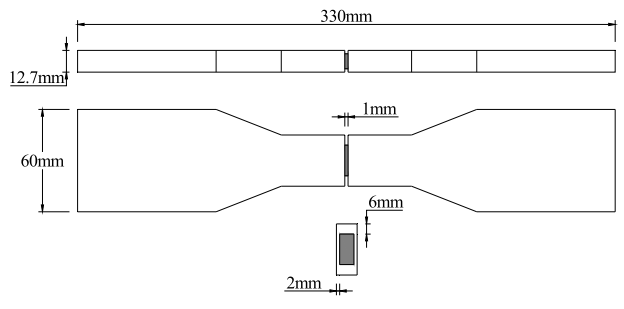


Fig. 6. Dimensions of notched dog-bone specimens.



Fig. 7. Uniaxial tension test setup on notched dog-bone specimens.

single crack. In order to capture the crack opening without including the deformation of the material adjacent to the crack, the gage length of LVDTs should be as small as possible, which is approximately 20 mm in this study. The notched dog-bone specimens were loaded to produce different crack widths ranging from $10\,\mu m$ to $110\,\mu m$, which is the most probable range of crack widths observed under preloading for each of the two ECC mixes used in this study. Once the predetermined extension of LVDTs was reached, the specimen was removed from the load frame and the single crack width was measured in the unloaded state. At least four specimens were tested for each crack width. The test was also conducted under displacement control at a rate of 0.5 mm/min.

After preloading, the specimens were exposed to wet-dry cycles for self-healing. The specimens were reloaded to failure after 10 healing cycles. The secant stiffnesses under preloading and reloading (defined in Section 4.2) were calculated, which were then used to compute the stiffness recovery $r_{\rm E}$ of each single crack specimen. The stiffness recovery as a function of crack width was determined from this data, and was subsequently used in the analytical scale-linking model.

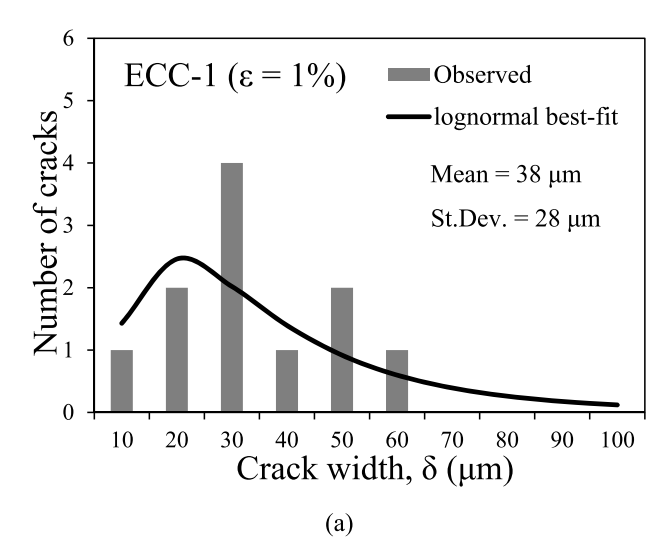
4. Experimental results and discussion

4.1. Crack widths distributions (macro-scale)

The observed crack patterns (average crack width and crack number within the gage length of 80 mm) of ECC-1 and ECC-2 are listed in

Table 2Crack patterns of ECC-1 and ECC-2 at various tensile strains.

ECC-1			ECC-2			
Strain (%)	Avg. crack width (μm)	Avg. no. of cracks	Strain (%)	Avg. crack width (µm)	Avg. no. of cracks	
0.25	21	4	0.3	17	3	
0.35	35	5	0.5	27	6	
0.5	33	6	0.8	32	9	
0.75	37	8	1.0	35	11	
1	38	10	1.2	33	13	
			1.5	36	14	
			1.8	45	17	
			2	53	17	



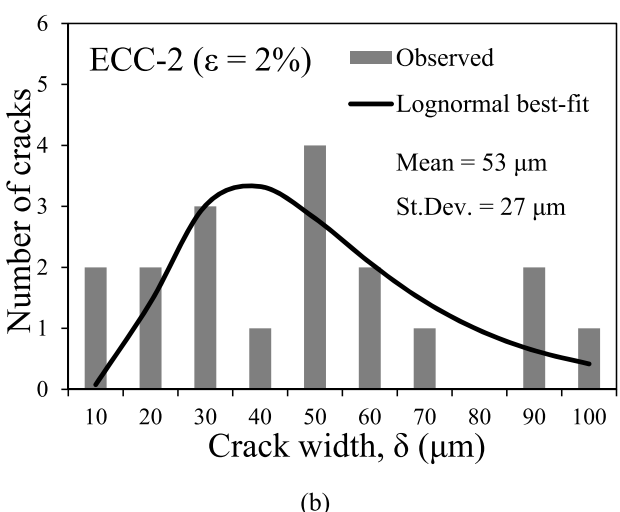


Fig. 8. Observed and lognormal best-fit of CWDs of (a) ECC-1 at strain of 1%, and (b) ECC-2 at strain of 2%.

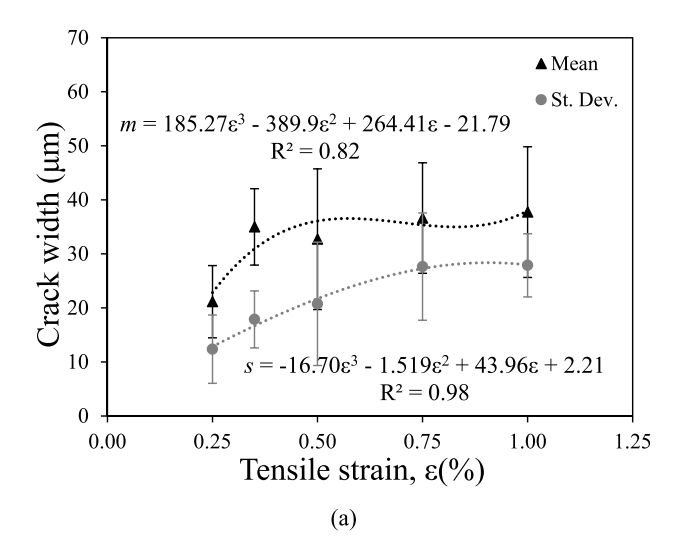
Table 2.

As can be seen, the crack width of ECC-1 is slightly larger than that of ECC-2 at the same tensile strains, while the crack number has the opposite trend. This can be attributed to the higher content of fly ash in the ECC-2 mixture. The un-hydrated fly ash with smooth spherical shape and small particle size increases the compactness of the interfacial transition zone between fiber and matrix, which increases the frictional bond strength. High frictional bond strength means a strong holding force in the interface and resistance to fiber sliding [36]. As a result, the crack width is smaller in ECC-2 compared to that of ECC-1. In addition, the multi-cracks are the source of tensile strain for ECC materials, therefore, ECC-2 has more cracks than ECC-1 at the same tensile strain due to the smaller crack width.

The typical observed CWDs of these two ECC materials at their highest preloading strain level, 1% for ECC-1 and 2% for ECC-2, are plotted in Fig. 8. Based on previous studies [27,28], the CWD of ECC can be fitted using a lognormal distribution. The corresponding lognormal distribution best-fit curves of the CWD are also shown in Fig. 8. The PDF of the lognormal distribution at a given strain level can be expressed as:

$$p(\delta, \varepsilon) = \frac{1}{\delta \sigma \sqrt{2\pi}} e^{\frac{-(\ln \delta - \mu)^2}{2\sigma^2}}$$
 (2)

where $p(\delta,\epsilon)$ is the probability of a given crack width δ being present in



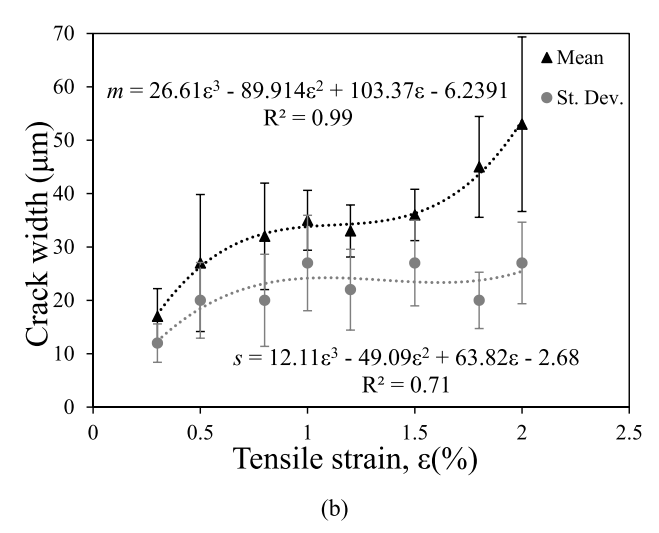


Fig. 9. Mean and standard deviation of CWD versus tensile strain for (a) ECC-1 and (b) ECC-2.

a ECC specimen at a given tensile strain $\epsilon.$ σ and μ are two parameters of PDF, which can be calculated using:

$$\mu = \ln\left(\frac{m^2}{m^2 + s^2}\right) \& \quad \sigma = \sqrt{\ln\left(\frac{s^2}{m^2} + 1\right)}$$
(3)

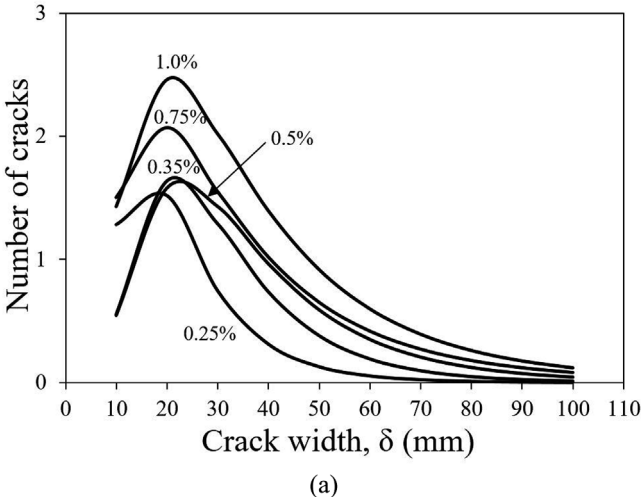
where m and s are the mean and standard deviation of crack widths at a given tensile strain, respectively.

These two parameters versus tensile strain of ECC-1 and ECC-2 are shown in Fig. 9. According to Ranade et al. [27] and Liu et al. [28], the data points of these parameters can be best fitted by cubic polynomial functions of tensile strain, as shown in Eqns. (4) and (5). Their corresponding regression equations are also presented in Fig. 9. Based on these two regression equations, the m and s can be computed at any tensile strain, so that the corresponding PDF of CWD can be obtained.

$$m = A_3 \varepsilon^3 + A_2 \varepsilon^2 + A_1 \varepsilon + A_0 \tag{4}$$

$$s = B_3 \varepsilon^3 + B_2 \varepsilon^2 + B_1 \varepsilon + B_0 \tag{5}$$

Using Equations (2)–(5), the CWDs at a given level of tensile strain of these two ECC mixtures can be uniquely described. Representative lognormal CWDs at various strain levels are plotted in Fig. 10. It should be noted that the best-fit curves were obtained by a scaling up the PDF of crack patterns at a particular strain level. It is meaningful only when the crack widths are in multiples of $10\,\mu m$, because the crack widths were recorded in intervals of $10\,\mu m$ as mentioned in Section 3.2.1.



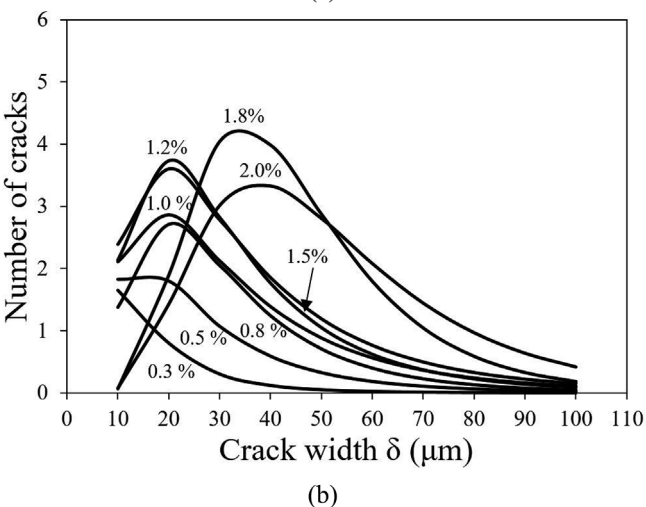


Fig. 10. Lognormal CWDs of (a) ECC-1 and (b) ECC-2 at various strain levels (the strain level was denoted next to the curves).

However, for the analytical scale-linking model in this study, the actual PDF was used, which is a continuous function for all crack widths. At this point, the macro-scale parameter $p(\delta,\epsilon)$ in the analytical scale-linking model has been obtained, and the details of meso-scale parameter r_E are described in next Section.

4.2. Stiffness recovery of single crack (meso-scale)

The secant stiffness ($E_{preloading}$ and $E_{reloading}$) of single crack specimens during preloading and reloading are defined in Fig. 11. The linear best-fit lines are drawn though the elastic range of the curves. For the preloading curve, the first cracking strength is the stress on the first drop point ($S_{preloading}$), while the stress value at the point of deviation is considered as the first cracking strength on the reloading curve ($S_{reloading}$). The secant stiffness is then defined as the slope between the origin and first cracking point.

It should be noted that the gage length of the LVDTs was 20 mm during tensile loading, which was larger than the notch thickness (1 mm). Therefore, the measured crack opening in Fig. 11 used to calculate the stiffness was not the true crack width of a single crack in the notched section. The measurement also contained the elastic deformation of the un-notched section within the gage of the LVDTs. In order to eliminate this influence, the true stiffness recovery as a function of crack width should be transferred from measured values. The details are shown in the following paragraphs.

The part of specimen within the gage length of the LVDTs was

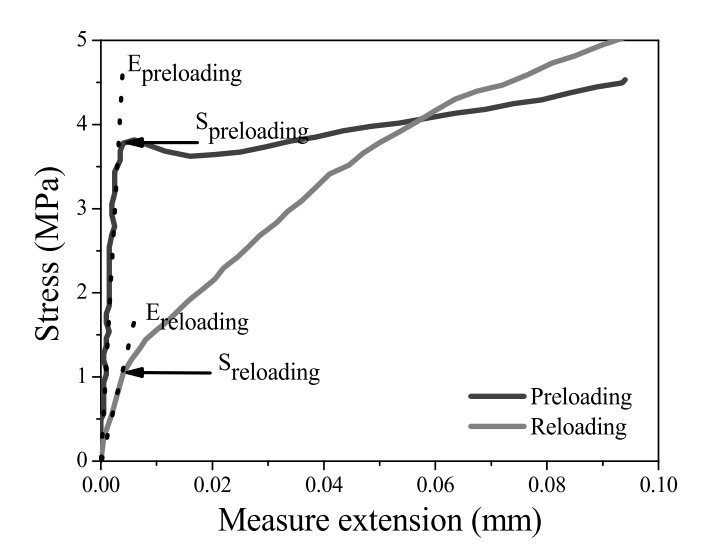


Fig. 11. Secant stiffness definition of single crack during preloading and reloading.

modeled as q+1 elements, and each element was assumed to have the same width (w = 1 mm) as the notch. Therefore, the measured crack opening δ_m during preloading can be expressed as:

$$\delta_m = \delta_{notch} + \delta_1 + \dots + \delta_q \tag{6}$$

The notched and un-notched section areas were defined as A_{notch} and A, respectively. Therefore, σ_{notch} equals to $\frac{A}{A_{notch}}\sigma$. Also, the initial stiffness of each element was defined as E_0 . With this, Eqn. (6) divided by σ_{notch} can be expressed as in Eqn. (7):

$$\frac{\delta_m}{\sigma_{notch}} = \frac{\varepsilon_{notch} w}{\sigma_{notch}} + \frac{q A_{notch}}{A} \frac{\varepsilon w}{\sigma} = \frac{w}{E_0} + \frac{q A_{notch}}{A} \frac{w}{E_0}$$
(7)

During reloading, a similar expression can be obtained as shown in Eqn. (8):

$$\frac{\delta'_m}{\sigma'_{notch}} = \frac{w}{E_{notch}} + \frac{qA_{notch}}{A} \frac{w}{E_0}$$
(8)

Combining Eqns. (7) and (8),

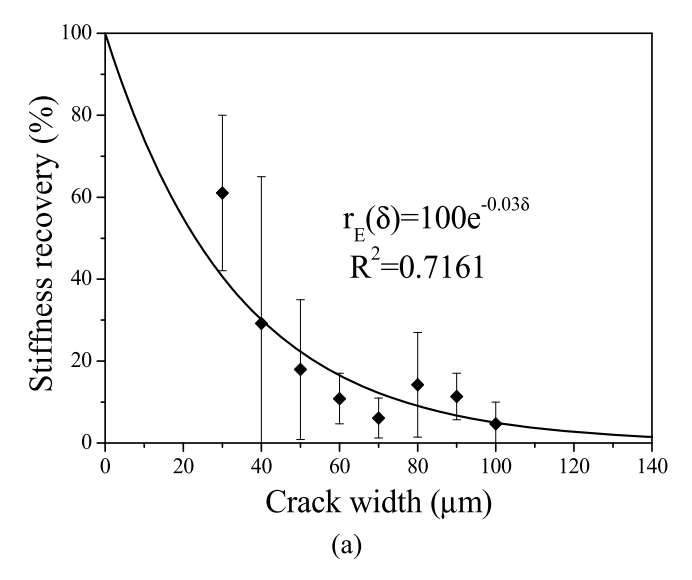
$$\frac{\delta_m \sigma'_{notch}}{\sigma_{notch} \delta'_m} = \frac{\frac{E_{notch}}{E_0} + \frac{qA_{notch}}{A} \frac{E_{notch}}{E_0}}{1 + \frac{qA_{notch}}{A} \frac{E_{notch}}{E_0}}$$
(9)

The left-hand side of this expression is the measured stiffness recovery of a single crack $r_c^m(\delta)$, while E_{notch}/E_0 is the true stiffness recovery $r_E^t(\delta)$ of a single crack. To simplify, $\frac{qA_{\text{notch}}}{A}$ can be defined as g. Hence, the true stiffness recovery $r_E^t(\delta)$ can be expressed as a function of measured stiffness recovery $r_E^m(\delta)$, as shown in Eqn. (10).

$$r_E^t(\delta) = \frac{r_E^m(\delta)}{1 + g - gr_E^m(\delta)} \tag{10}$$

Using this equation, the true stiffness recovery of a single crack as a function of crack width can be obtained as shown in Fig. 12. In theory, the stiffness recovery should be 100% when the crack width is zero, and cannot be negative even at infinite crack width. Therefore, the exponential function is appropriate to best-fit the experimental data points of stiffness recovery. As can be seen, the stiffness recovery was found to decrease exponentially as crack width increases, for both ECC-1 and ECC-2.

According to Fig. 12, self-healing of ECC occurs if crack width is limited to below 140 µm and the specimen is exposed to at least 10 wet/dry cycles exposure regime, consistent with the findings of Li and Yang [37]. However, the results of previous studies using resonant frequency and permeability measurements suggested that crack-damaged ECC specimens can be healed completely when the crack width falls below



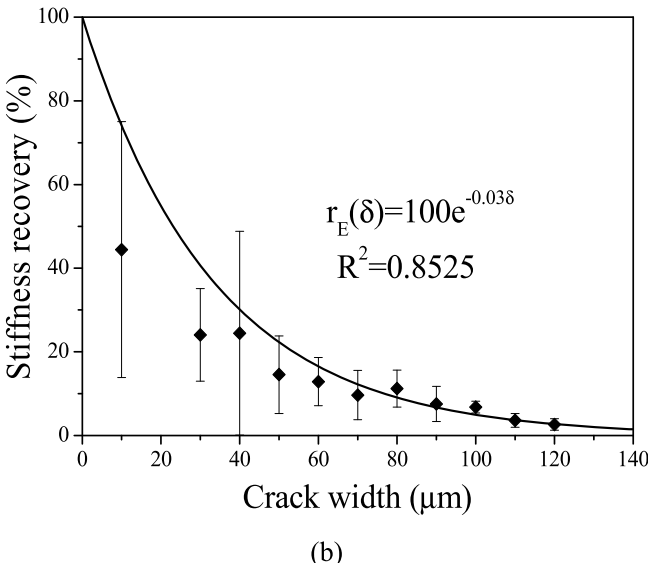


Fig. 12. Stiffness recovery of single crack as a function of crack width for (a) ECC-1, and (b) ECC-2.

 $50\,\mu m$ [18,38,39,40]. In this study, the measured stiffness recovery shows large variations from 15 to 75% recovery at the crack width of $10\,\mu m$. This may be a result of self-healing products which are a combination of C-S-H and calcium carbonate, with lower stiffness compared with ECC matrix before cracking. Further, self-healing is more effective near specimen surface than interior [44], which could lead to a higher level of recovery when measured by permeability or resonant frequency compared with stiffness recovery. Therefore, the stiffness recovery of 100% is not likely to occur in real practice.

The corresponding regression equations are also presented in Fig. 12. The regression equation of ECC-1 was found to be the same as that of ECC-2, which means that the stiffness recovery as a function of crack width is the same for these two ECC materials used in this study. Although ECC-1 and ECC-2 have different mix proportions (especially the fly ash to cement ratio), the stiffness recovery of a single crack is essentially the same at any given crack width. This indicates that the crack width is the dominating influence factor of stiffness recovery due to self-healing, independent of the exact material compositions, at least for these two ECCs studied.

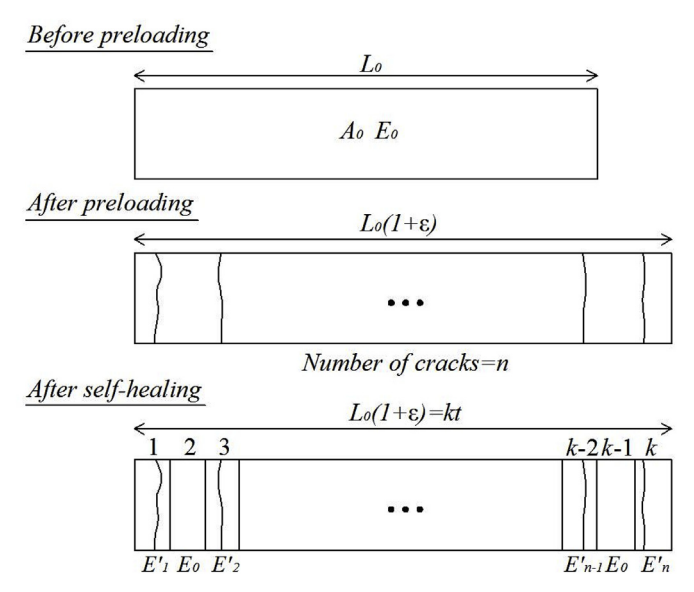


Fig. 13. Schematic representation of the methodology of the analytical scalelinking model.

5. Scale-linking model development and verification

5.1. Scale-linking model

The analytical scale-linking model described in this section utilizes the crack width probability density function $p(\delta, \varepsilon)$ (macro-scale) and the single crack stiffness recovery function $r_E^t(\delta)$ (meso-scale) to predict the stiffness recovery level of ECC as a function of tensile strain. The detailed methodology of the scale-linking model is shown schematically in Fig. 13. Prior to preloading, the ECC composite (rectangular middle section of a dog-bone specimen) has the initial stiffness E0, cross sectional area A₀, and length L₀. When the ECC specimen is preloaded to an imposed strain level ε , n micro cracks with various crack widths are produced. After preloading, the specimen is modeled as k elements, where the stiffness of the specimen is assumed to act as k springs in series. Each element has length t equal to 3 mm, smaller than the theoretical minimum crack spacing of ECC materials derived in Ref. [35] [41]. This element size ensures that each element can contain only a single crack, so that the elements can represent the experimentally obtained stiffness recovery data discussed in Section 4.2.

The stiffness of a cracked element is defined as E_i after being self-healed. For the un-cracked elements (k-n), the stiffness after self-healing is assumed to be E_0 , which is the same as the initial value. Based on classical mechanics, the composite stiffness $E^{'}$ after self-healing can be expressed as:

$$E' = \frac{k}{\sum_{i=1}^{n} \frac{1}{E_i'} + \sum_{n=1}^{k} \frac{1}{E_0}} = \frac{k}{\sum_{i=1}^{n} \frac{1}{E_i'} + \frac{(k-n)}{E_0}}$$
(11)

The stiffness recovery of a single crack r_E as a function of crack opening δ can be defined as in Eqn. (12), which has been determined experimentally in Section 4.2.

$$r_E(\delta) = \frac{E'(\delta)}{E_0} \tag{12}$$

If the CWDs are considered discrete and the number of cracks with crack width of δ_i is n_i , then Eqns. (11) and (12) can be combined as:

$$E' = \frac{k}{\sum_{i=1}^{n} \frac{1}{E_i'} + \frac{(k-n)}{E_0}} = \frac{k}{\sum_{j} \frac{n_j}{E'(\delta_j)} + \frac{(k-n)}{E_0}} = \frac{kE_0}{\sum_{j} \frac{n_j}{r_E(\delta_j)} + (k-n)}$$
(13)

However, in reality, the CWDs are not discrete and crack widths can have a value between zero and infinity following a PDF $p(\delta,\epsilon)$, which

has been determined experimentally in Section 4.1. Therefore, the number of cracks n_j (with crack width of δ_j) can be expressed as in Eqn. (14), and Eqn. (13) can then be re-expressed as Eqn. (15).

$$n_{i} = np(\delta_{i}, \varepsilon)d\delta \tag{14}$$

$$E' = \frac{kE_0}{\sum_j \frac{np(\delta_j, \epsilon)d\delta}{r_E(\delta_j)} + (k - n)} = \frac{kE_0}{n\left(\int_0^\infty \frac{p(\delta, \epsilon)}{r_E(\delta)}d\delta - 1\right) + k}$$
(15)

For ECC materials, the deformation in tension is caused by multiple cracks and the elastic deformation of the matrix is negligible compared to crack width. Therefore, the total crack number n can be calculated as the total deformation (ϵL_0) divided by the mean crack width as shown in Eqn. (16).

$$n = \frac{\varepsilon L_0}{\int_0^\infty \delta p(\delta, \varepsilon) d\delta}$$
 (16)

The number of elements k can be calculated as shown in the following equation:

$$k = \frac{L_0(1+\varepsilon)}{t} \tag{17}$$

Therefore, by combining Eqn. (14) through (17), the analytical scale-linking model to predict the composite stiffness recovery $R_E(\epsilon)$ as function of tensile strain can be derived as follows:

$$R_{E}(\varepsilon) = \frac{E'}{E_{0}} = \frac{(1+\varepsilon)}{\int_{0}^{\infty} \delta p(\delta,\varepsilon)d\delta} \left(\int_{0}^{\infty} \frac{p(\delta,\varepsilon)}{r_{E}(\delta)}d\delta - 1\right) + (1+\varepsilon)$$
(18)

Based on the PDF $p(\delta,\epsilon)$ of CWD and stiffness recovery of single crack $r_E(\delta)$ determined experimentally in Section 4, the scale-linking model allows prediction of the composite stiffness recovery of ECC under a certain strain level ϵ using Eqn. (18). It should be noted that because the crack widths were measured in the unloaded state, they had a rebound of 15% compared to the true crack widths under loading [18]. Therefore, the tensile strain ϵ in Eqn. (18) includes a reduction coefficient of 0.85.

In order to verify the analytical scale-linking model derived above, the experimental composite stiffness recovery should be investigated and compared with predicted values. The details of comparison are described in the following sections.

5.2. Comparison of analytical and experimental results

Once the crack patterns and stiffness recovery of a single crack were obtained, the analytical scale-linking model could predict macro-scale stiffness recovery of both ECC-1 and ECC-2 at various tensile strains, as shown in Fig. 14. As can be seen in this figure, the analytical scalelinking model predicted curves for both ECC have a similar shape. The stiffness recovery reduces rapidly at lower tensile strains (< 0.75% for ECC-1 and < 1% for ECC-2), and it reduces gradually in the middle tensile strains (0.75–1.25% for ECC-1 and 1%–2% for ECC-2). When the tensile strain gets close to the tensile strain capacity of each ECC mixture, the stiffness recovery reduces drastically again. A probable cause for this result is the fact that the crack width has the dominant effect on stiffness recovery, as described in Section 4.2. The average crack width of ECC increases rapidly at lower tensile strain ranges, but stabilizes at higher tensile strain ranges when the number of cracks increases [29]. However, when the tensile strain approaches its capacity, more and more fibers are ruptured and pulled out and, as a result, the crack width increases again.

It also can be seen that the composite stiffness recoveries of both ECC materials predicted by analytical scale-linking model generally agree with the experimental data. This indicates that the scale-linking model proposed in this study successfully links meso- and macro-scales stiffness recovery and can be used to predict the stiffness recovery of ECC due to self-healing at any tensile strain.

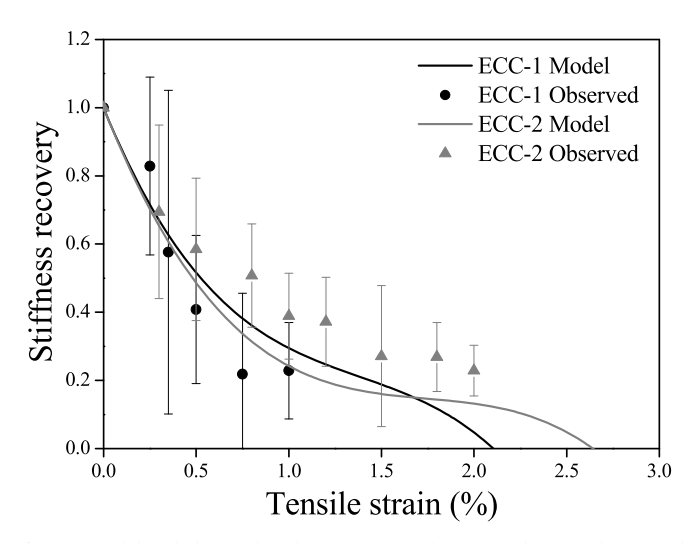


Fig. 14. Model and observed stiffness recovery of ECC-1 and ECC-2 show rapid decay with strain at lower strain range, slower decay at higher strain range, until close to failure strain when the stiffness recovery becomes negligible.

The probable cause for the deviations between the model and experimental data is the fact that the accuracy of the handheld microscope used in this study leads to errors in measuring crack widths. As mentioned previously, the microscope measured the crack widths in intervals of $10\,\mu m$. Therefore, some cracks with a width below $10\,\mu m$ might not be captured. Even when cracks were captured, their crack widths were rounded to $10\,\mu m$ when recording data. In addition, other crack widths between intervals of $10\,\mu m$ might be over or under estimated. For example, a crack with actual width of $23\,\mu m$ might be recorded as 20 or $30\,\mu m$. This error can be reduced by using higher precision measurement technology, such as high resolution cameras and the digital image software recommended in Ref. [27] [42].

It is well known that the crack widths in ECC are reduced on specimen unloading at a given strain. However, the exact reduction percentage may differ for different ECC materials, and requires further investigation. To simplify, the reduction percentage of 15% was used for both ECC-1 and ECC-2 in this study, which probably causes the underestimated model prediction for the ECC-2.

In addition, the variation of crack width along a single crack is another probable reason for the discrepancies observed. In reality, the crack width along the crack is not constant. In this study, the crack widths at four points along each crack were measured, and their average value was taken as the crack width used in the analytical scale-linking model. In spite of this, this method could not reflect the actual crack patterns at specific tensile strain. This error can be reduced by more careful crack width measurement and testing a larger number of specimens.

Even though the single crack test intends to study the stiffness recovery of a single crack, ECC have an intrinsic tendency to develop multiple cracking in the interior of the notched specimen [43]. The single crack stiffening recovery function, therefore, may suffer in accuracy from this phenomenon.

According to Fan and Li [44], the crack width and the self-healing ability along the crack depth are not constant. However, only surface crack patterns were used in this study. The crack patterns and the influence of self-healing on stiffness recovery in the interior of the specimen were not taken into account in this study. More detailed and accurate investigations will be conducted in future studies using computed tomography (CT) scan for internal crack width measurements.

6. Conclusions

An analytical scale-linking model, linking the stiffness recovery on

the meso-scale to that on the macro-scale, was proposed and verified experimentally. Based on the research findings, the following conclusions can be drawn:

- (1) The analytical scale-linking model successfully quantifies the relationship between self-healing at the composite level and that at the single crack level. The model captures essential information of crack width distribution in a composite and crack width dependency of stiffness recovery at the single crack level.
- (2) Self-healing, as measured by recovery of stiffness, is dominated by crack width, and less so by the material composition, at least within the limited range of material ingredient variation (ECC-1 versus ECC-2) used in this study.

As a result of this study, from a robust self-healing viewpoint, it is preferred to design an ECC composite with larger number of cracks with smaller crack width, when loaded to a given strain in the strain-hardening state.

The proposed model can be used to predict the magnitude of stiffness recovery of different parts of a structure subjected to applied loading, as long as the spatial distribution of tensile strain is known and assuming the same environmental condition (wet-dry cycles) as adopted in this model exists for self-healing. For other environmental exposure conditions, for example, under continuous water immersion, the stiffness recovery function $r_{\rm E}$ (δ) must be experimentally determined for the single crack specimen under this condition, prior to using the proposed model.

Acknowledgements

Support from the US National Science Foundation (Grant CMMI 1634694) to the University of Michigan is gratefully acknowledged. The authors also acknowledge the material suppliers Headwaters Resources (Fly ash) and Kuraray (PVA fiber) for providing materials used in this study.

References

- [1] G.B. Jacobsen, S.J. Marchand, Concrete crack I: durability and self-healing a review, The 2nd International Conference on Concrete under Severe Conditions, Environment and Loading, 1998, pp. 217–231.
- [2] B.H. Oh, S.W. Cha, B.S. Jang, S.Y. Jang, Development of high-performance concrete having high resistance to chloride penetration, Nucl. Eng. Des. 212 (1–3) (2002) 221–231.
- [3] K.R. Lauer, F.O. Slate, Autogenous healing of cement paste, ACI J. Proc. 52 (6) (1956) 1083–1098.
- [4] D. Snoeck, N.D. Belie, From straw in bricks to modern use of microfibers in cementitious composites for improved autogenous healing a review, Construct. Build. Mater. 95 (2015) 774–787.
- [5] E. Cuenca, L. Ferrara, Self-healing capacity of fiber reinforced cementitious composites. State of the art and perspectives, KSCE J. Civ. Eng. 21 (7) (2017) 2777–2789
- [6] S. Granger, A. Loukili, G. Pijaudier-Cabot, G. Chanvillard, Experimental characterization of the self-healing of cracks in an ultra high performance cementitious material: mechanical tests and acoustic emission analysis, Cement Concr. Res. 37 (4) (2007) 519–527.
- [7] K. Wang, D.C. Jansen, S.P. Shah, A.F. Karr, Permeability study of cracked concrete, Cement Concr. Res. 27 (3) (1997) 381–393.
- [8] M.D. Lepech, V.C. Li, Water permeability of engineered cementitious composites, Cement Concr. Compos. 31 (10) (2009) 744–753.
- [9] J. Cowie, F.P. Glasser, The reaction between cement and natural waters containing dissolved carbon dioxide, Adv. Cem. Res. 4 (15) (1992) 119–134.
- [10] H. Ma, S.Z. Qian, Z.G. Zhang, Effect of self-healing on water permeability and mechanical property of medium-early-strength engineered cementitious composites. Construct. Build. Mater. 68 (2014) 92–101.
- [11] N. Ter Heide, Crack Healing in Hydrating Concrete, Delft University of Technology, 2005.
- [12] Z.G. Zhang, S.Z. Qian, H. Ma, Investigating mechanical properties and self-healing behavior of micro-cracked ECC with different volume of fly ash, Construct. Build. Mater. 52 (2014) 17–23
- [13] C. Edvardsen, Water permeability and autogenous healing of cracks in concrete, ACI Mater. J. 96 (4) (1999) 448–454.

- [14] V.C. Li, From micromechanics to structural engineering the design of cementitious composites for civil engineering application, J. Struct. Eng. Earthq. Eng. 10 (2) (1993) 37–48.
- [15] V.C. Li, Engineered cementitious composites (ECC) tailored composites through micromechanical modeling, Can. Soc. Civ. Eng. (1997) 1–38.
- [16] V.C. Li, On engineered cementitious composites (ECC). A review of the material and its applications, J. Adv. Concr. Technol. 1 (3) (2003) 215–230.
- [17] K. Yu, Y. Wang, J. Yu, S. Xu, A strain-hardening cementitious composites with the tensile capacity up to 8%, Construct. Build. Mater. 137 (2017) 410–419.
- [18] Y.Z. Yang, M.D. Lepech, E.H. Yang, V.C. Li, Autogenous healing of engineered cementitious composites under wet-dry cycles, Cement Concr. Res. 39 (5) (2009) 382–390
- [19] L.L. Kan, H.S. Shi, A.R. Sakulich, V.C. Li, Self-healing characterization of engineered cementitious composite materials, ACI Mater. J. 107 (6) (2010) 617–624.
- [20] E.N. Herbert, V.C. Li, Self-healing of microcracks in engineered cementitious composites (ECC) under a natural environment, Materials 6 (7) (2013) 2831–2845.
- [21] B. Hilloulin, F. Grondin, M. Matallah, A. Loukili, Modelling of autogenous healing in ultra high performance concrete, Cement Concr. Res. 61–62 (2014) 64–70.
- [22] B. Hilloulin, D. Hilloulin, F. Grondin, A. Loukili, N.D. Belie, Mechanical regains due to self-healing in cementitious materials: experimental measurements and micromechanical model, Cement Concr. Res. 80 (2016) 21–32.
- [23] A. Aliko-Benítez, M. Doblaré, J.A. Sanz-Herrera, Chemical-diffusive modeling of the self-healing behavior in concrete, Int. J. Solid Struct. 69–70 (2015) 392–402.
- [24] R. Davies, A. Jefferson, Micromechanical modelling of self-healing cementitious materials, Int. J. Solid Struct. 113–114 (2017) 180–191.
- [25] A. Caggiano, V. Krelani, L. Ferrara, G. Etse, Zero-thickness interface formulation for fracture analysis of self-healing concrete, 1st Pan-American Congr. Comput. Mech. PANACM 2015 11th Argentine Congr, Comput. Mech. MECOM 1 (2015) 553–564.
- [26] G. Di Luzio, L. Ferrara, V. Krelani, Numerical modeling of mechanical regain due to self-healing in cement based composites, Cement Concr. Compos. 86 (2018) 190–205.
- [27] R. Ranade, J. Zhang, J.P. Lynch, V.C. Li, Influence of micro-cracking on the composite resistivity of engineered cementitious composites, Cement Concr. Res. 58 (2014) 1–12.
- [28] H.Z. Liu, Q. Zhang, C.S. Gu, H.Z. Su, V.C. Li, Influence of micro-cracking on the permeability of engineered cementitious composites, Cement Concr. Compos. 72 (2016) 104–113.
- [29] V.C. Li, S.X. Wang, C. Wu, Tensile strain-hardening behavior of polyvinyl alcohol engineered cementitious composite (PVA-ECC), ACI Mater. J. 98 (6) (2001) 483–492.
- [30] V.C. Li, C. Wu, S.X. Wang, A. Ogawa, T. Saito, Interface tailoring for strain-hardening polyvinyl alcohol-engineered cementitious composite (PVA-ECC), ACI Mater. J. 99 (5) (2002) 463–472.
- [31] H. Ma, S.Z. Qian, Z.G. Zhang, Z. Lin, V.C. Li, Tailoring engineered cementitious composites with local ingredients. Construct. Build. Mater. 101 (2015) 584–595.
- [32] Japan Society of Civil Engineers, Recommendations for Design and Construction of High Performance Fiber Reinforced Cement Composites with Multiple Fine Cracks, HPFRCC, 2008, p. 82.
- [33] Z.G. Zhang, S.Z. Qian, V.C. Li, Ductile concrete material with self-healing capacity for jointless concrete pavement use, Transp. Res. Rec. J. Transp. Res. Board. 2640 (2017) 78–83
- [34] I. Paegle, G. Fischer, Evaluation of Standardized Test Methods to Characterize Fiber Reinforced Cement Composites, in SHCC2, December 2011 9–16.
- [35] E.B. Pereira, G. Fischer, J.A.O. Barros, Direct assessment of tensile stress-crack opening behavior of strain hardening cementitious composites (SHCC), Cement Concr. Res. 42 (6) (2012) 834–846.
- [36] E.H. Yang, Y.Z. Yang, V.C. Li, Use of high volumes of fly ash to improve ECC mechanical properties and material greenness, ACI Mater. J. 104 (6) (2007) 620–628.
- [37] V.C. Li, E.H. Yang, Self-healing in concrete materials, in: S. van der Zwaag (Ed.), In Self Healing Materials: an Alternative Approach to 20 Centuries of Materials Science, Springer, 2007, pp. 161–193.
- [38] D. Snoeck, Self-healing and Microstructure of Cementitious Materials with Microfibres and Superabsorbent Polymers, Ghent University, 2016.
- [39] D. Snoeck, N. De Belie, Repeated autogenous healing in strain-hardening cementitious composites by using superabsorbent polymers, J. Mater. Civ. Eng. 4015086 (2015) 1–11.
- [40] D. Snoeck, K. Van Tittelboom, S. Steuperaert, P. Dubruel, N.D. Belie, Self-healing cementitious materials by the combination of microfibres and superabsorbent polymers, J. Intell. Mater. Syst. Struct. 25 (1) (2014) 13–24.
- [41] H.C. Wu, V.C. Li, Snubbing and bundling effects on multiple crack spacing of discontinuous random fiber-reinforced brittle matrix composites, J. Am. Ceram. Soc. 75 (12) (1992) 3487–3489.
- [42] G.P.A.G. van Zijl, V. Slowik, R.D. Toledo Filho, F.H. Wittmann, H. Mihashi, Comparative testing of crack formation in strain-hardening cement-based composites (SHCC), Mater. Struct. 49 (4) (2016) 1175–1189.
- [43] J. Yu, C.K.Y. Leung, Novel experimental method to determine crack-bridging constitutive relationship of SHCC using digital image processing, International Conference on Strain-hardening Cement-based Composites, SHCC4), 2017, pp. 55–62.
- [44] S. Fan, M. Li, X-ray computed microtomography of three-dimensional microcracks and self-healing in engineered cementitious composites, Smart Mater. Struct. 24 (1) (2015) 15–21.